Electronic structure of amorphous Si measured by (e,2e) spectroscopy

1995 J. Phys.: Condens. Matter 7 279

(http://iopscience.iop.org/0953-8984/7/2/006)

J. Phys.: Condens. Matter 7 (1995) 279–288. Printed in the UK

Electronic structure of amorphous Si measured by (e, 2e) spectroscopy

M Vos, P Storer, Y Q Cai, A S Kheifets, I E McCarthy and E Weigold†
Electronic Structure of Materials Centre, Flinders University of South Australia, GPO Box 2100, Adelaide, SA 5001, Australia

Received 12 July 1994, in final form 21 September 1994

Abstract. Energy-resolved electron momentum densities are determined for a thin Si film evaporated onto a carbon foil. This is done by transmission (e, 2e) spectroscopy, a technique that does not rely on crystal momentum and is therefore ideally suited for the study of amorphous materials. Spectra were collected with an energy resolution of 2 eV and a momentum resolution of 0.15 au (0.3 $Å^{-1}$). The main feature disperses in a strikingly similar way to the crystalline ones. In addition to the dispersion the intensities of the peaks are obtained. In spite of having only a qualitative understanding of the shape of the spectra, the results of the comparison of measured amorphous momentum densities with calculated crystalline ones are reasonable. The basis of this agreement between *amorphous* solid and *crystalline* theory is discussed.

1. Introduction

Amorphous (or 'glassy') solids, especially amorphous semiconductors, have received considerable interest in recent years, both because of technological importance, and becuse it is a challenge to describe these materials theoretically in a proper way. In a crystal the translational symmetry simplifies calculations greatly, and theories are formulated in terms of crystal momentum k with $k = q + G$, where G is a reciprocal lattice vector and q the real electron momentum. As early as 1971 Ziman attempted to describe amorphous semiconductors such as Si or Ge as a 'perturbed crystal' and derived a 'band structure' of amorphous solids, using bond orbitals [1]. This 'band structure' is reproduced, in a slightly modified form (drawn in the extended-zone scheme) in figure 1. The conclusion of Ziman's argument was that near the top and bottom of the valence band there is a dispersion relation between energy and momentum similar to a perfect crystal, but in the middle the band is broadened because of the lattice disorder. The present paper describes the direct observation of the energy–momentum density of the valence electrons of amorphous silicon using electron momentum spectroscopy based on the (e, 2e) reaction. For each bound electron in an ensemble the complete kinematics of an ionization reaction is observed, enabling its real momentum and binding energy to be determined. Factors that make the observations imperfect are described below the description of the experiment. This new technique is ideally suited to observe the dispersion relation (and in addition the corresponding electron density) for amorphous solids. We verify that the dispersion relation in amorphous Si is indeed close to the crystalline one and we set an upper limit to the broadening of the 'band structure'.

† Present address: Research School of Physical Sciences and Engineering, Australian National University, Canberra, ACT 0200, Australia.

0953-8984/95/020279+10$19.50

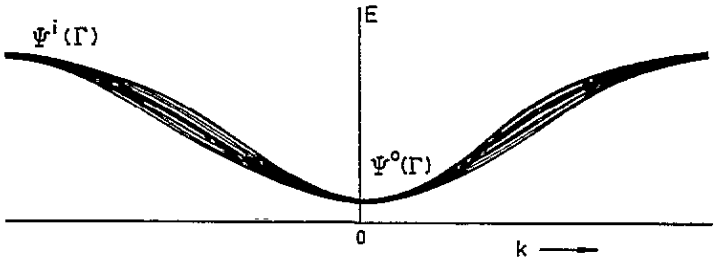

Figure 1. Qualitative sketch of the relation between momentum and binding energy as predicted by Ziman for amorphous silicon or germanium.

The (e, 2e) technique differs from earlier observations of densities of states in energy or momentum in that it directly measures the energy density for each momentum, and the momentum density for each energy. Photoelectron spectroscopy (e.g. [2]) gives information about the energy density. Compton scattering [3] gives information about momentum density in one direction, integrated over the other momentum directions and energy. The energy–momentum (dispersion) relation can often be inferred from angle-resolved photoelectron spectroscopy (for Si see e.g. [4]) under the assumption of a single crystal with a flat surface, but it cannot be applied to the question of dispersion in amorphous solids.

Because of the extremely thin targets necessary for (e, 2e), it is not yet possible to perform an (e, 2e) experiment on crystalline or polycrystalline silicon and thus to compare energy–momentum densities for different forms. In the present work we confine ourselves to answering the question raised by Ziman about the dispersion for amorphous silicon. Integrated techniques show only small differences between amorphous and crystalline silicon [2, 3]. Comparisons between amorphous and crystalline forms have been made for carbon in an (e, 2e) experiment using the present spectrometer [5, 6]. Significant differences in the energy–momentum densities were observed for amorphous carbon, annealed amorphous carbon and highly oriented pyrolitic graphite (HOPG). However the momentum-integrated energy distributions showed negligible differences. From this we conclude that integrated techniques are not sufficiently sensitive to observe these differences.

It should be noted that the radial distribution function, as measured by diffraction techniques, is much broader for amorphous carbon [7] than for amorphous silicon [8]. Amorphous silicon has a quite well defined nearest-neighbour distance, with the second-nearest-neighbour distance varying because of deviations of the bond angles from the ideal tetrahedral one [9]. In amorphous carbon the order is considerably less, and hence larger deviations of the electronic structure are expected. Another possible reason is the presence of both sp^2 and sp^3 hybridization in this case. It is therefore expected that the differences between the electronic structure of crystalline silicon and amorphous silicon are much smaller than those found for the case of carbon.

In an (e, 2e) measurement an incoming electron ionizes the target and the scattered and ejected electrons are detected in coincidence. A well collimated monoenergetic electron beam (energy E_0, momentum k_0) impinges on a target. Some of these electrons will be scattered over large angles by a collision with a target electron. In the case of high-momentum-transfer collisions this process is well described as a binary collision between the scattered and ejected (target) electrons and is quantitatively well understood [10]. Due to the energy transfer the target electron is ejected. We detect both scattered and ejected electrons *in coincidence* and determine their energies and momenta (E_s and k_s for the slower electron, E_f and k_f for the faster one). We choose atomic units with $\hbar = 1$ thereby equating

momentum and wave numbers. A comparison of the momentum and energy of the scattered and ejected electron with the momentum and energy of the incident electron gives us the magnitude of the momentum and binding energy of the ejected electron *before* the collision. At high enough energies the electrons can be treated as plane waves. We can determine the binding energy ε as

$$\varepsilon = E_0 - E_s - E_f \tag{1}$$

and the recoil momentum q, which in the plane-wave impulse approximation is equal and opposite to the momentum of the target electron before the collision:

$$q = k_0 - k_s - k_f. \tag{2}$$

Thus a complete description of the kinematics of the ionizing event is obtained. In this paper momentum is expressed in atomic units. 1 atomic unit is 1.89 Å^{-1}.

For crystals this technique should be able to measure the dispersion law $\varepsilon(k)$, where k is usually restricted to the first Brillouin zone. One obtains the value of k by adding the appropriate reciprocal lattice vector G to q. It should work for polycrystalline solids in the same way as for single crystals (obtaining of course an angular average in the former case). More significantly it should be able to obtain the relation between real electron momentum q and binding energy in an amorphous solid, where the concept of crystal momentum does not apply.

2. Experimental details

In our spectrometer we use the simultaneous detection of multiple energies and azimuthal angles in both detectors in order to shorten the data acquisition time. Extensive details of this spectrometer are given elsewhere [11]. The spectrometer is shown schematically in figure 2. An asymmetric geometry was chosen, as the Mott cross-section for electron–electron scattering is strongly peaked in the forward direction, with $E_0 = 20$ keV, $E_s \simeq 18.8$ keV, scattering angle 14°, $E_s \simeq 1.2$ keV, angle 76°. This resulted in count rates of several hundreds of true coincidences a minute for amorphous carbon films of 80 Å thickness and a data-acquisition time of a few days for a complete set of spectra.

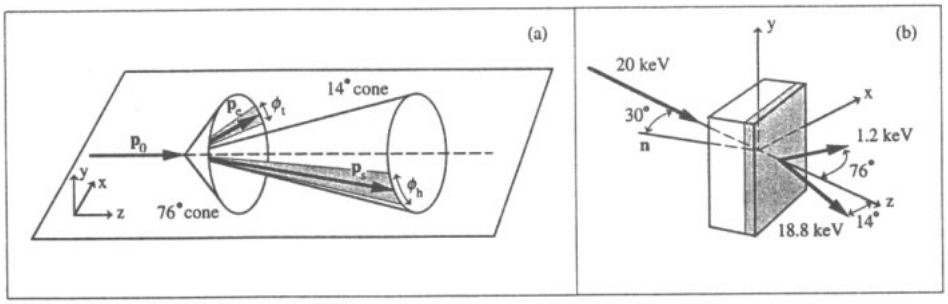

Figure 2. In (a) the experimental geometry is outlined. Both scattered and ejected electrons are detected over a range of azimuthal angles. The direction of the momentum of the detected electrons is roughly along the y axis. In (b) we show the orientation of the samples relative to the electron beams involved. Due to the low mean free path of the 1.2 keV electrons only (e, 2e) events occurring in the evaporated silicon layer (hatched) have an appreciable chance of being detected without further energy loss.

Under these experimental conditions the momentum components perpendicular to the surface cancel, and the measured momentum is in the plane of the surface (y direction). An

additional property of the asymmetric set-up is the fact that one of the outcoming electrons has rather low energy. This electron has by far the lowest elastic and inelastic mean free paths, and it determines the depth over which information from the target is obtained. In our case 35 Å of silicon was evaporated on an amorphous carbon backing of 80 Å and is indicated as the shaded layer in figure 2. Room-temperature deposition is known to result in amorphous silicon [8]. The evaporated thickness was determined from a crystal-thickness monitor. The effective thickness of this layer is 50 Å, because the outgoing angle for the slow (as well as for the fast) electron was 45°. The estimated inelastic mean free path for an electron at 1.2 keV is 22 Å and the elastic mean free path is 15 Å. Thus the direct contribution of the carbon backing (assuming a homogeneous coverage) is suppresed by a factor of about 250 compared to its intensity before the evaporation. The vacuum during evaporation was 3×10^{-9} Torr. After the evaporation the sample was transferred under vacuum to the main chamber with a pressure of $\simeq 2.5 \times 10^{-10}$ Torr during the actual measurement.

The sample-preparation method described above should be applicable to all materials that can be evaporated, and do not have a strong tendency to form islands on an amorphous carbon backing. Samples prepared in this way should have relatively clean surfaces. It is an easy way to prepare a wide variety of suitable (e, 2e) targets. Historically the thickness required for (e, 2e) targets has limited its use almost exclusively to carbon films [12, 13, 14]. The surface sensitivity of the present set-up may also allow the study of surface effects. Of course these samples will be either polycrystalline or amorphous. The preparation of suitable single-crystal samples will require more complicated procedures.

3. Results and discussion

In figure 3 we show a set of (e, 2e) spectra for the different momentum intervals indicated. Any carbon contributing to the spectra would cause a peak around 27 eV below the vacuum level for zero momentum [5]. However even this most intense feature is still buried in the noise. We will assume thus that, within statistical accuracy, all intensity is due to the silicon overlayer. The raw data were deconvoluted for inelastic energy loss using a smooth function peaking around 20 eV energy loss. Because both carbon and silicon contribute to the loss function and three electrons with different trajectories and energies have to be taken into account, it is not easy to obtain this function experimentally. It is therefore not possible to derive the deconvolution parameters in a rigorous way, as has been done for pure carbon samples in [15]. As carbon has a broad plasmon loss feature with maximum intensity $\simeq$25 eV energy loss (depending on its density) and Si has maximum energy loss at $\simeq$15 eV, we choose a smooth loss function with a maximum around 20 eV. The amount of deconvolution was determined empirically, so the intensity well below the bottom of the silicon valence band is approximately equal to zero. The spectra of different momenta were deconvoluted with exactly the same parameters, and the general low value of the intensity at high binding energy gives some confidence in the procedure followed. Different shape response functions will redistribute the intensity of the spectra to some extent, but will not affect the derived peak positions severely. The main feature is a peak around 17 eV (below the vacuum level) for zero momentum, slowly dispersing towards lower binding energy with increasing momentum.

In order to compare this behaviour with the one expected for crystalline silicon (unfortunately no (e, 2e) measurements of crystalline silicon are available to date) we plot the calculated momentum densities of angular-averaged crystalline silicon in the same plot. These calculations were obtained using a linear-muffin-tin orbital (LMTO) approach [16].

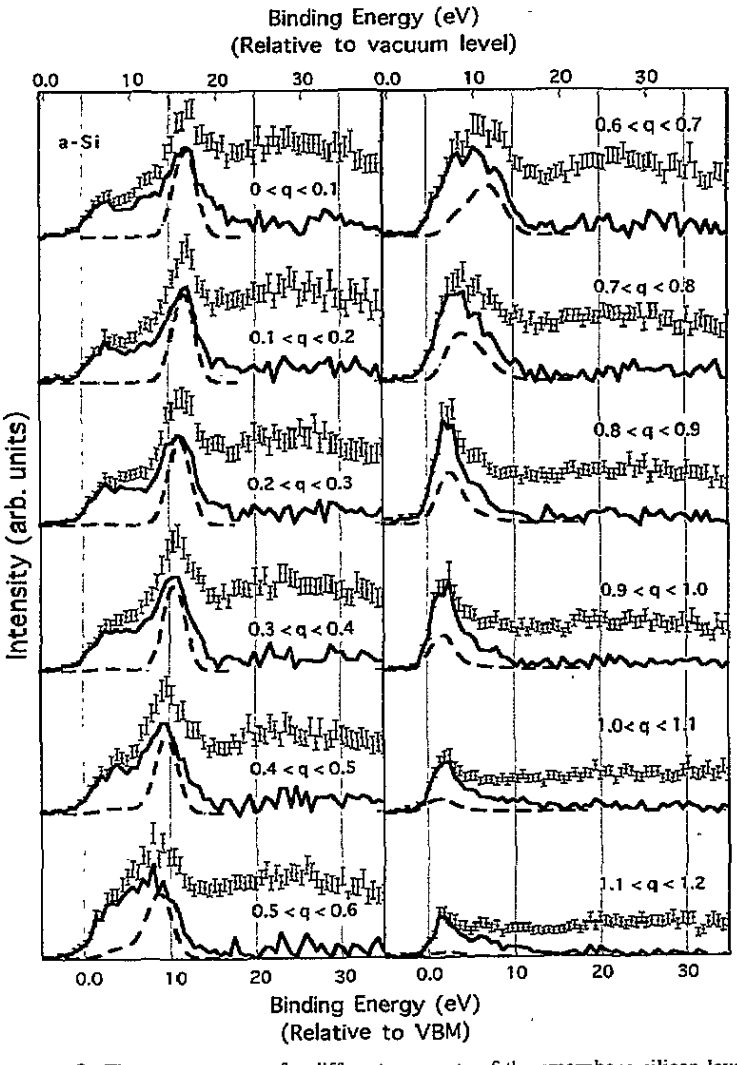

Figure 3. The energy spectra for different momenta of the amorphous silicon layer. The raw data (error bars) have been deconvoluted (full lines) from (e, 2e) events with plasmon excitation. The calculated angular-averaged momentum densities of crystalline silicon are plotted as broken lines. Note that the strongest feature of C is a peak at 22 eV below the Fermi level and is not visible at all in these spectra.

Results were convoluted by a Gaussian of 3 eV full width at half maximum, in order to facilitate comparison with experiment. Only part of this 3 eV is due to experimental broadening, as we measured the width of the carbon 1s core level under similar experimental conditions to be 2 eV [17]. Experimental binding energies are obtained relative to the vacuum level, whereas the calculation is relative to the valence-band maximum (VBM). The position of the valence-band maximum was estimated to be between 4 and 4.5 eV below the vacuum. This was inferred from the onset of the experimental spectra at this value for high momentum ($\simeq$1 au). Clearly the experimental dispersion for amorphous silicon and the theoretical dispersion for crystalline silicon are very similar.

The measured and experimental dispersion are once more compared in figure 4. In

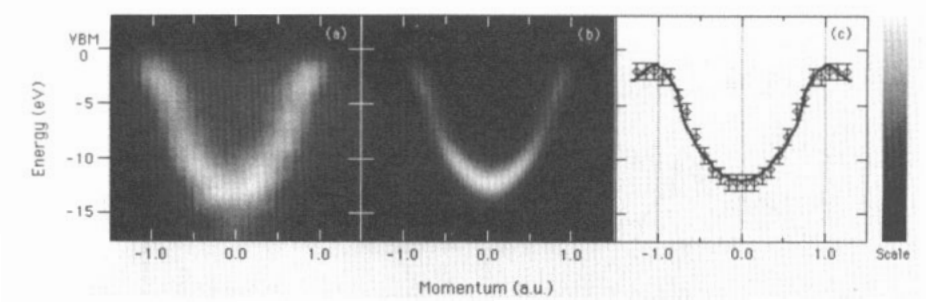

Figure 4. The measured electron energy–momentum distribution for the amorphous silicon layer (a). The lighter the shading the higher the intensity. Note the qualitative similarity with figure 1. In (b) we plot the calculated intensity (averaged over all crystal directions and broadened with the experimental energy and momentum resolution) in a similar fashion. In (c) we compare the measured dispersion relation with the one obtained from this calculation.

figure 4(a) we show the experimental measured intensity (after deconvolution) as a grey scale plot. The points with highest intensity have the lightest shading. Notice the qualitative resemblance with figure 1. Thus the prediction made by Ziman in 1971 [1] that the dispersion in an amorphous semiconductor resembles the crystalline one is verified. In figure 4(b) we show the theoretical calculation, convoluted with momentum and energy resolution, in a similar plot. The calculated 'image' of the valence band and the measured 'image' resemble each other nicely. The dispersion of the momentum with energy was determined from the energy position of the feature with highest intensity as determined from spectra as plotted in figure 3. This is shown in figure 4(c) together with a theoretical estimate. Note the excellent agreement between theory and experiment.

Having verified that the dispersions of the amorphous and crystalline solids are quite similar, we now turn to the question of whether we can determine the degree of 'fuzziness' of the dispersion relation due to the lattice disorder. Unfortunately our experiment has finite momentum and energy resolution (estimated to be respectively 0.15 au and 2 eV). Thus this determination is not a trivial one. From figure 1 we see that the excess width is largest where the dispersion is steepest. This means that the best way to attempt to determine the width is by studying the momentum-density plots as a function of energy. The finite energy resolution does not contribute much to the width of the momentum plots at energies other than near the bottom of the band because binding energy changes quickly with momentum. These plots are shown in figure 5 for the deconvoluted data. Also plotted in this figure is the theoretical estimate of the momentum densities. Excellent agreement is obtained for the peak positions. The main discrepancy is the intensity at small binding energies near zero momentum. This is of course the same excess intensity as we discussed in the energy spectra of figure 3. We have no clear indication of any excess width in the momentum peaks. So we estimate that the maximum fuzziness due to the disorder is less than 0.15 au (0.3 $Å^{-1}$).

Let us now focus on the big differences between the experimental and theoretical results. Most noticably there is a lot of intensity at binding energies lower than the main feature. It is tempting to attribute this to the amorphous nature of the sample. However (e, 2e) experiments done with the same spectrometer on crystalline graphite films show a similar behaviour [5, 6]. This is especially clear in the energy-resolved momentum-density plots as shown for selected energies for both silicon and annealed (i.e. partly recrystallized) evaporated carbon and HOPG as shown in figure 6. The binding energies of the silicon and carbon samples were chosen in such a way that the separation of the momentum peaks is

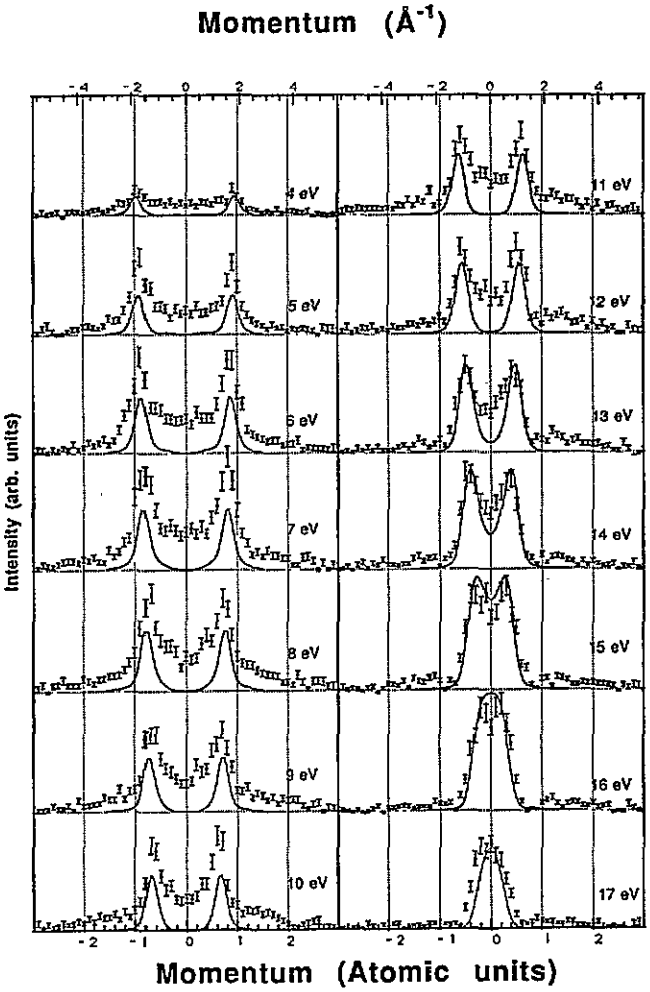

Figure 5. The measured intensity as a function of electron momentum for different energies as indicated. Also shown are the densities obtained from the band structure calculations after broadening with the momentum and energy resolution.

approximately the same for both cases. We suggest that the general equivalent shape of all three densities shows that the same physics governs the shape of all three densities. In all three cases there is a significant intensity between the peaks corresponding to the dispersing bands, whereas outside these peaks, the intensity drops quickly to zero. In principle this intensity between the band peaks could have three causes.

(i) It is a true reflection of the momentum density, but (for example because we measure near the surface) the momentum density is *not* properly described by the band structure calculations. If this were the case one would expect this intensity to change if one changed the surface sensitivity of the experiment, by changing the angle with the surface of the slow electrons. Experimental tests for the case of annealed evaporated carbon show that variations in shape with exit angle, if present at all, are very minor.

(ii) It is due to 'satellite structures' which affect the energy balance of equation (1). Satellite structures usually show up at the high-binding-energy side (i.e. away from the Fermi

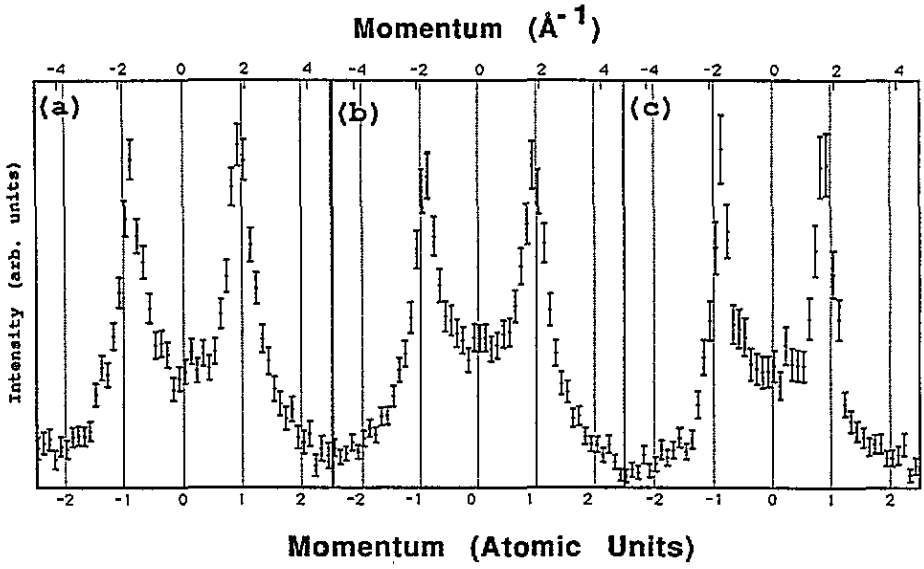

Figure 6. A comparison of the momentum densities of HOPG (a), annealed evaporated carbon (b) and amorphous silicon (c). A binding energy (relative to the vacuum level) of 18 eV for the two carbon densities and of 6 eV for the silicon one was chosen because their momentum peaks have similar separation. Notice the similar shapes of the densities, with all of them having a significant intensity at zero momentum, suggesting that these shapes have the same physical origin.

level) of the main peak. From figure 3 we see that the main excess intensity is at the low-binding-energy side. We should be careful however because we could have removed a lot of satellite intensity at the high-binding-energy side by the somewhat arbitrary deconvolution procedure. Assuming that the excess intensity is due to satellites (with no momentum changes due to these satellites) it could be correct to compare the total area of the measured deconvoluted spectra of figure 3 with the theoretical densities as shown in figure 3. The satellites would then only cause a redistribution of the intensity within the same momentum bin. This comparison is plotted in figure 7(a). Measurement and calculations agree quite well, although we want to stress that we have no justification for attributing the intensity at lower binding energy and small momentum to a 'satellite structure'.

(iii) It could be due to elastic scattering through an appreciable angle of one of the electrons involved. This will affect the momentum balance of equation (2) and hence causes the inference of the wrong target electron momentum. We want to stress the vector nature of momentum here. The spectrometer measures target-electrons with momentum along the y direction (figure 2), assuming no multiple scattering. Additional momentum transfer due to elastic multiple scattering has a number of possible effects on the (e, 2e) events measured. These are (a) a target electron with momentum along the y axis is ejected and its (e, 2e) event is detected but the wrong momentum is calculated (although it is still along the y axis), (b) an electron with momentum along the y axis is ejected but because of elastic scattering its momentum as inferred from equation (2) is not along the y axis any longer, and hence cannot be detected, (c) a target electron with its momentum not directed along the y axis is ejected, but due to elasic scattering its (e, 2e) event is detected, and it is wrongly inferred that the original momentum was along the y axis. Thus this case is considerably more complicated than the energy-loss one. There is a clear asymmetry in the

density plots of figure 5 (i.e. there is more excess intensity on the low-momentum side of the peaks than on the high-momentum side). This can be attributed to the vector nature. Many different initial states with the same value of $|q|$ (and hence approximately the same binding energy) can, after small-angle elastic-scattering events of one of the electrons involved in the (e, 2e) event, contribute to the intensity near zero momentum. At larger momenta than the main peaks small-angle scattering is sufficient for only those initial states with q already pointing in about the right direction.

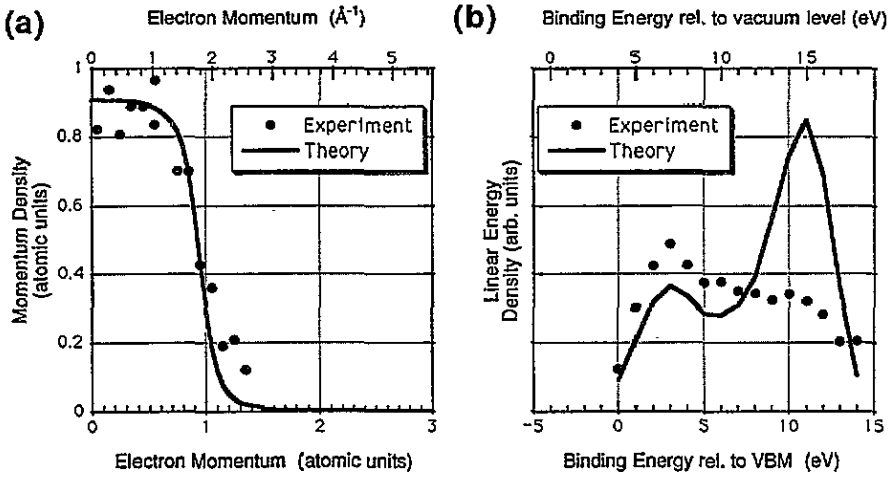

Figure 7. A comparison of the experimental and theoretical densities. In (a) we plot the momentum density a function of energy from the areas shown in figure 3. In (b) we plot the linear energy density as a function of momentum from the areas as plotted in figure 5.

Thus because of the vector nature of momentum we cannot say that elastic scattering would merely cause a redistribution of the measured intensity of the energy-resolved momentum-density plots as shown in figure 5. Still the dependence of the ratio of the measured and calculated areas as shown in figure 5 may provide a clue to this puzzle. These 'linear energy densities of states' are shown in figure 7(b). Both experiment and theory show a maximum around 3 eV below the valence-band maximum while the experiment has considerably less intensity at high binding energies. These energies correspond to the bottom of the band i.e. around zero momentum. Note that for zero momentum scattering of type iii(c) does not exist, so we cannot add spurious momentum by elastic scattering in that case. This may be the reason why the curve is relatively low at these energies.

In principle the true energy density of states could be obtained from figure 5 by weighting them with a q^2. In practice this is difficult because the integration has to be extended to high momentum values before convergence is obtained. Well before this momentum value is reached (up to 4 au according to the calculations!) the experimental intensity is much smaller than their error bars. Thus although agreement is less good for case (iii) than case (ii) the deviation found is the one expected if events of type iii(c) are important. Reasonable agreement could probably be obtained if we took the area in the sharp peaks at low binding energies (discarding the contaminated (e, 2e) events, mainly of type iii(c) in the middle) and take all intensity at the bottom of the band (where events of type iii(c) do not contribute), with some intermediate approach in between. At present we have not developed a method to do this without an excess of arbitrary assumptions. We are proposing to calculate them. Looking at figure 5 this approach, especially if we succeed in improving the momentum

resolution, could well turn out to be feasible.

4. Conclusion

In summary we have measured energy-resolved momentum densities in amorphous silicon. We have shown that the main intensity disperses in a way strikingly similar to crystalline silicon. With our present resolution we can only set an upper limit to the broadening of the band structure of 0.15 au. Calculations of the energy momentum densities for a bulk crystal are compared with the ones measured for the amorphous form. The present experiment raises some questions in the context of the (e, 2e) technique. Why are the observed densities in the high-momentum tail larger than the ones calculated by the independent-particle model for a bulk crystal? We believe the differences to be significant, although this conclusion might change when we improve the energy and momentum resolution of the spectrometer. The momentum distribution could conceivably be broadened by diffuse scattering. This can be tested by comparing targets with different silicon thicknesses. Experience with (e, 2e) reactions in the gas phase [10] has shown that one cannot trust the higher-momentum components from independent-particle calculations. To what extent the momentum broadening is an effect due to the amorphous nature will be tested, among other things, by future experiments on crystalline silicon. These questions, and others, suggest that (e, 2e) spectroscopy of silicon is a fruitful field for future experiments that will become possible with further development of the technique.

Acknowledgments

The authors want to thank the technical staff of the Electronic Structure of Materials Centre for their indispensable contributions to the construction of the (e, 2e) spectrometer. The Electronic Structure of Materials Centre is supported by a grant of the Australian Research Council.

References

[1] Ziman J M 1971 *J. Phys. C: Solid State Phys.* **4** 3129
[2] Ley L, Kowalczyk S, Pollak R and Shirley D A 1972 *Phys. Rev. Lett.* **29** 1088
[3] Bonse U, Schulke W and Wolf G 1980 *Phil. Mag.* B **42** 499
[4] Wachs A L, Miller T, Shapiro T C and Chiag A P 1985 *Phys. Rev.* B **32** 2236
[5] Vos M, Storer P J, Canney S, Kheifets A S, McCarthy I E and Weigold E 1994 *Phys. Rev.* B **50** 5635
[6] Vos M, Storer P J, Cai Y Q, McCarthy I E and Weigold E 1994 *Phys. Rev.* B (15 December issue)
[7] Robertson J 1986 *Adv. Phys.* **35** 317 and references therein
[8] Roorda S, Sinke W C, Poate J M, Jacobson D C, Dierker S, Dennis B S, Eaglesham D J, Spaepen F and Fuoss P 1991 *Phys. Rev.* B **44** 3702
[9] Lannin J S 1988 *Phys. Today* **41** 28
[10] McCarthy I E and Weigold E 1991 *Rep. Prog. Phys.* **54** 789
[11] Storer P J, Clark S A C, Caprari R C, Vos M and Weigold E 1994 *Rev. Sci. Instrum.* **65** 2214
[12] Ritter A L, Dennison J R and Jones R 1984 *Phys. Rev. Lett.* **53** 2054
[13] Gao C, Ritter A L, Dennison J R and Holzwarth N A W 1988 *Phys. Rev.* B **37** 3914
[14] Hayes P, Williams J F and Flexman J 1991 *Phys. Rev.* B **43** 1928
[15] Jones R and Ritter A L 1986 *J. Electron. Spectrosc. Relat. Phenom.* **40** 285
[16] Skriver H L 1984 *The LMTO Method* (Berlin: Springer)
[17] Caprari R S, Clark S A C, McCarthy I E, Storer P, Vos M and Weigold E 1994 *Phys. Rev.* B **50** 12078